Organic Electronics 13 (2012) 7–12

Contents lists available at SciVerse ScienceDirect

Organic Electronics

journal homepage: www.elsevier.com/locate/orgel

Nanostructure effect of V_2O_5 buffer layer on performance of polymer-fullerene devices

Cheng Gong [a,b], Hong Bin Yang [a], Qun Liang Song [a,b], Chang Ming Li [a,b,]*

[a] School of Chemical and Biomedical Engineering and Center for Advanced Bionanosystems, Nanyang Technological University, 70 Nanyang Drive, Singapore 637457, Singapore
[b] Institute for Clean Energy & Advanced Materials, Southwest University, Chongqing 400715, PR China

ARTICLE INFO

Article history:
Received 30 July 2011
Received in revised form 20 September 2011
Accepted 3 October 2011
Available online 20 October 2011

Keywords:
Nanostructure
Polymer solar cell
V_2O_5 nanobelt

ABSTRACT

Nanostructure of solar cell materials is often essential for the device performance. V_2O_5 nanobelt structure is synthesized with a solution process and further used as an anode buffer layer in polymer solar cells, resulting insignificantly improved power conversion efficiency (*PCE* of 2.71%) much higher than that of devices without the buffer layer (*PCE* of 0.14%) or with V_2O_5 powder as the buffer layer (1.08%). X-ray diffraction (XRD) results indicate that the V_2O_5 nanobelt structure has better phase separation while providing higher surface area for the P3HT:PCBM active layer to enhance photocurrent. The measured impedance spectrums show that the V_2O_5 nanobelt structure has faster charge transport than the powder material. This work clearly demonstrates that V_2O_5 nanobelt has great potential as a substitute of the conventionally used PEDOT-PSS buffer layer for high performance devices.

1. Introduction

Polymer solar cells have attracted much attention due to their potential for low cost and large area solar cell devices [1–8]. The most widely studied polymer solar cell is composed of a layer of poly(3-hexylthiophene) (P3HT)/phenyl-C61-butyric acid methyl ester (PCBM) bulk heterojunction (BHJ) sandwiched between a transparent ITO anode and a metal cathode [9–16]. During illumination, excitons are generated in the P3HT:PCBM layer and further dissociated into free charges driven by the different energy levels of P3HT and PCBM followed by being transported to ITO anode and metal cathode for collection. In the process the electrical contacts between the P3HT:PCBM layer and the two electrodes have a critical effect on the device characteristics such as short-circuit current density (J_{sc}), open-circuit voltage (V_{oc}), fill factor (*FF*) and power conversion efficiency (*PCE*). Modification of the electrodes using inorganic or organic charge transport buffer layer is a common way to improve the contacts between the BHJ layer and electrodes. Poly (3,4-ethylene-dioxythiophene)-poly (styrene sulfonic acid) (PEDOT-PSS) is the most widely used material to modify the ITO anode as the buffer layer [17]. However, numerous studies have shown that PEDOT-PSS is not suitable for mass production of polymer solar cells due to the intrinsic acid and hygroscopic properties [18]. Therefore, alternative materials such as WO_3, NiO, Cs_2CO_3, V_2O_5 and MoO_3 have been developed [19–22]. Sol–gel deposited V_2O_5, MoO_3 and WO_3–V_2O_5 mixed oxides have been used to modify the anode in organic electronics recently [23,24]. In particular, these transition metal oxides like MoO_3, WO_3, and V_2O_5 have been proven that they are actually *n*-type semiconductors with very deep lying conductive band and a high work function [25,26]. A very recent work even shows that V_2O_5 has a huge work function of 7 eV [27]. Therefore, they are not electron blocking material. V_2O_5 is one of those transition metal

---

* Corresponding author at: Nanyang Technological University, School of Chemical and Biomedical Engineering, Center for Advanced Bionanosystems, 70 Nanyang Drive, Singapore 637457, Singapore. Fax: +65 67911761.

E-mail address: ECMLi@ntu.edu.sg (C.M. Li).

1566-1199/$ - see front matter © 2011 Elsevier B.V. All rights reserved.
doi:10.1016/j.orgel.2011.10.006

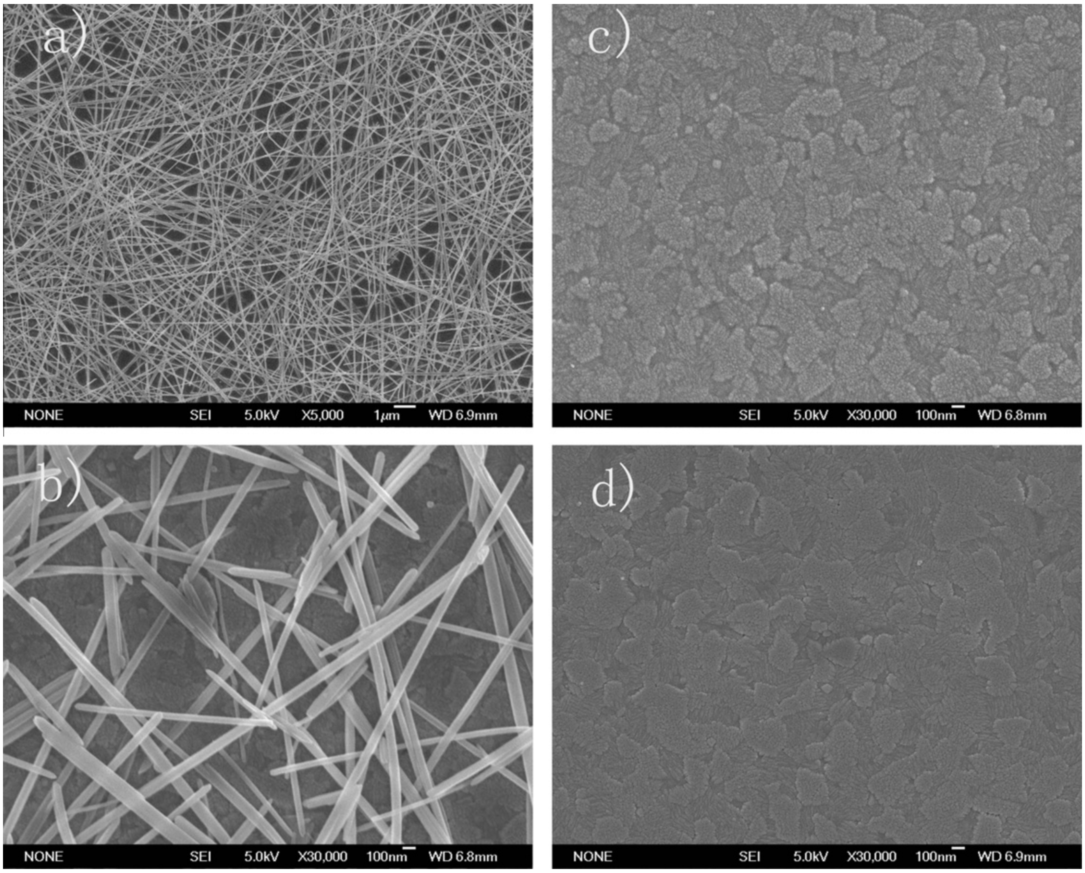

Fig. 1. FESEM image of the (a) V_2O_5 nanobelt film, (b) V_2O_5 nanobelt on ITO substrate, (c) V_2O_5 powder on ITO substrate and (d) ITO substrate.

oxides explored as the buffer layer in polymer solar cells with both normal structure and inverted structure [19,22], in which V_2O_5 is deposited on the substrate by thermal evaporation method, which is unfavorable for mass production. Solution-processed V_2O_5 has been employed as an anode interlayer in a polymer solar cell with an inverted structure [28], demonstrating 40% *PCE* improvement. However, the effect of V_2O_5 nanostructure as a buffer layer on device performance has not been studied. In this work, V_2O_5 nanobelts are synthesized with a solution process and further used as an anode buffer layer in normal structure polymer solar cell devices. The XRD and impedance results are compared with devices comprising a V_2O_5 powder buffer layer to study the performance enhancement mechanism of the nanobelt structure.

2. Experimental

V_2O_5 nanobelts were prepared by a hydrothermal method [29]. Typically, V_2O_5 powder (0.364 g, Aldrich-223794, >98%) and 30 mL H_2O were mixed at room temperature followed by adding 5 mL 30% H_2O_2 to produce a transparent orange solution. The resultant solution was then transferred to a 60 mL autoclave and kept in an oven at 200 °C for 3 days. The product was washed with anhydrous ethanol and distilled water several times. Finally, it was dried at 80 °C in vacuum for 6 h. The synthesized products were characterized by a field emission scanning electron microscope (FESEM, JSM-6700F).

To fabricate polymer solar cell devices, the V_2O_5 nanobelt or V_2O_5 powder with various concentrations in isopropanol (IPA) was ultrasonicated to form a pale yellow solution. The solution was spin-coated on top of a pre-cleaned ITO patterned glass substrate at 1000 rpm for 30 s. P3HT (Aldrich) blended with PCBM (American Dye Source) were dissolved in chlorobenzene (with concentration of 20 and 16 mg/mL, respectively) and spin coated onto the V_2O_5 nanobelt layer at 1000 rpm for 30 s. After that, the devices were transferred into vacuum ($<1.5 \times 10^{-5}$ Pa) for the thermal deposition of aluminum electrodes (100 nm). After devices fabrication, thermal annealing was carried out in vacuum at 150 °C before the characteristic current–voltage (*I*–*V*) curves were measured by Keithley 2420 under illumination of a Newport solar simulator with AM 1.5G filter. All the fabrication and measurement processes except the aluminum electrode deposition were carried out in air at room temperature.

The X-ray diffractograms (XRD) samples (measured by Bruker AXS D8 Advance) were fabricated by the same procedure of fabricating solar cell devices except that the Al electrodes were not deposited on top of the P3HT:PCBM

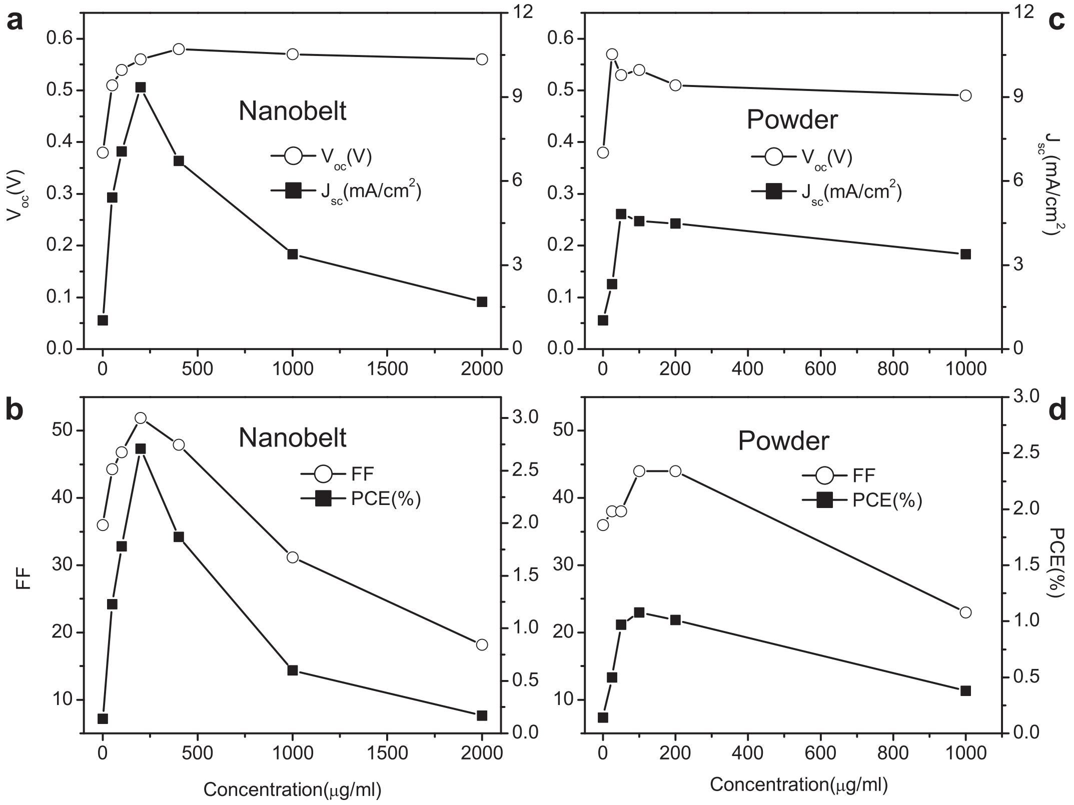

Fig. 2. Relationship of photovoltaic parameters (V_{oc}, J_{sc}, FF and PCE) versus V_2O_5 nanobelt (a and b) and powder (c and d) concentration (μg/mL).

layer. The concentration of V_2O_5 powder and V_2O_5 nanobelt for XRD samples are 200 μg/mL. Two samples with only V_2O_5 powder and V_2O_5 nanobelt on top of ITO were fabricated for comparison.

3. Results and discussion

The FESEM images of free standing V_2O_5 nanobelt film and V_2O_5 nanobelt formed on ITO surface are shown in Fig. 1, illustrating that the products are composed of a large quantity of nanobelt with typical lengths up to tens of micrometers (Fig. 1a). The nanobelts are flexible and have smooth surfaces. Higher resolution images (not shown here) show that the width and the thickness of these nanobelts are around 100 and 20 nm, respectively. After V_2O_5 nanobelts are dissolved in isopropanol and spin coated on ITO surface, they become shorter in length (Fig. 1b). The SEM sample in Fig. 1b was prepared by spin coating a low concentration of V_2O_5 nanobelt (5 μg/mL) onto ITO surface for non-full coverage, which gave clear images of the nanobelts. V_2O_5 powder was also dissolved in IPA (50 μg/mL) and spin coated on ITO to obtain SEM images for comparison. As shown in Fig. 1c and d, the surface morphology of V_2O_5 powder film is relatively smooth almost the same as that of ITO. Obviously, the V_2O_5 nanobelt film is much rougher than that of power V_2O_5 film and ITO surface. This result agrees with the reported AFM images of V_2O_5 powder sample [28].

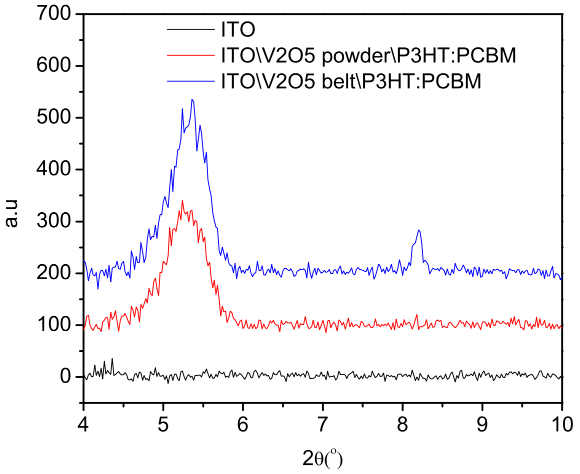

Fig. 3. X-ray diffraction results of different ITO/P3HT:PCBM with V_2O_5 nanobelt and V_2O_5 powder as buffer layer.

The concentrations of V_2O_5 nanobelt and powder were optimized respectively to achieve the highest *PCE*. The results show that with the V_2O_5 nanobelt concentration J_{sc}, V_{oc}, and *FF* increase until the highest *PCE* of 2.71% achieves at the concentration of 200 μg/mL, then decrease follow (Fig. 2a and b). V_2O_5 powder devices exhibit a similar trend, in which with increase of the V_2O_5 powder concentration

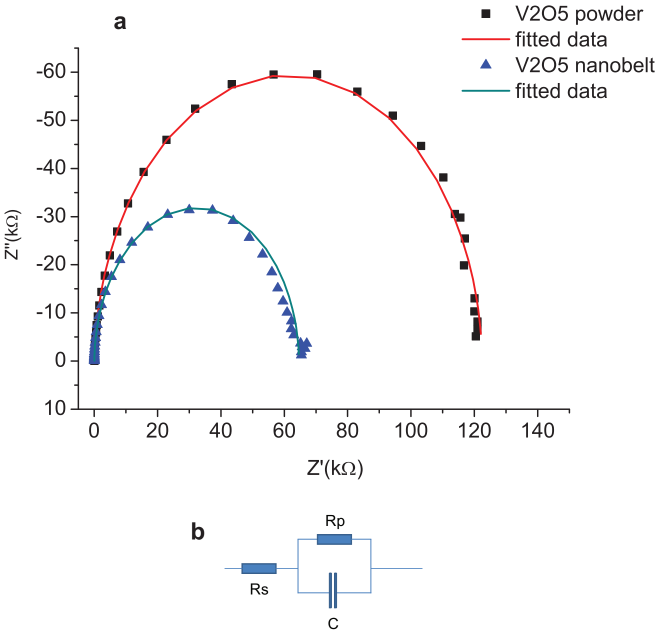

Fig. 4. (a) The ac impedance responses of the devices with V_2O_5 powder (black), V_2O_5 nanobelt (red) and PEDOT-PSS (blue) as the buffer layer. (b) The equivalent diagram of the devices. (For interpretation of the references to colour in this figure legend, the reader is referred to the web version of this article.)

the device *PCE* increases until reaching the maximum 1.08% at 100 μg/mL, then decreases also follows (Fig. 2c and d). The effect of V_2O_5 as a buffer layer on a polymer solar cell performance is understandable. V_2O_5 has been recently reported by Meyer et al. to have as high work function as 7.0 eV, indicating that it is a very efficient hole-injector due to the dipole at the V_2O_5-organic layer interface [27]. The dipole could efficiently extract holes from the active layer for better solar cell performance [24]. However, at low concentrations, no enough V_2O_5 nanobelts or powder covers the surface of ITO electrode as shown by the SEM images in Fig. 1b. That is why the *PCE* increases with increase of the V_2O_5 concentration. However, after the nanobelts or power fully cover the ITO electrode surface to achieve the maximum *PCE*, further increase of the V_2O_5 concentration leads to more than one layer of V_2O_5 nanobelt or powder on the ITO electrode surface, which could cause high resistance of hole transport to decrease in photocurrent J_{sc} and *PCE* as well. When the concentration of V_2O_5 is larger than 1000 μg/mL, devices eventually cannot work possibly due to either high resistance of the whole cell.

Although the devices with V_2O_5 powder as the buffer layer considerably improves *PCE* in powder devices from 0.14% to 1.08%, they cannot compete with V_2O_5 nanobelt-buffered devices with the highest *PCE* of 2.71%. In particular, the V_2O_5 powder buffered devices have much lower J_{sc} and *FF* than that of the nanobelts-buffered devices. X-ray diffraction (XRD) was characterized to study the reason of higher J_{sc} of V_2O_5 nanobelt devices compared to that of V_2O_5 powder devices in Fig. 3. No peak over a range of 4–10° is observed for the surfaces of bare ITO, V_2O_5 powder on ITO and V_2O_5 nanobelt on ITO. The peaks at $2\theta = 5.4°$ in both V_2O_5 powder and V_2O_5 nanobelt-buffered P3HT:PCBM samples correspond to the reflection of spacing between P3HT lamellae. The peak at $2\theta = 8.2°$ only observed in the V_2O_5 nanobelt-buffered device is the crystal domain of PCBM [30]. This indicates that V_2O_5 nanobelt buffer enhances the crystallinity and phase separation in the P3HT:PCBM film. It has been reported that enhanced phase separation could lead to the increase of J_{sc} [12,31]. Therefore, the better J_{sc} of V_2O_5 nanobelt devices is contributed from the enhanced phase separation in the active layer.

Impedance spectra were measured as shown in Fig. 4a to study the hole transport properties of V_2O_5 as the buffer layers, each of which shows a semicircles and can be fitted by the equivalent circuit shown in Fig. 4b, which comprises series resistance (*Rs*), parallel resistance (*Rp*) and capacitance (*C*) of the devices. The fitted data in Table 1 show that *Rs* and *C* do not have significant difference. However, the charge transport resistance (*Rp*) of the nanobelt-buffered device is significantly lower than the powder-buffered one, indicating that former has much faster charge transport rate than the latter. The time constant ($T \equiv \mathrm{Rp} \times C$) are 409 and 209 μs for V_2O_5 powder and V_2O_5 nanobelt based devices, respectively. A shorter time constant means that charge can move faster to reach the electrode for reducing the charge recombination process [32], thus resulting in larger photocurrent. Obviously, the

Table 1
The series resistance (*Rs*), parallel resistance (*Rp*), capacitance (*C*) and time constant (*T*) extracted from the fitted data.

	Rs (Ω)	*C* (nF)	*Rp* (Ω)	*T* (μs)
V_2O_5 nanobelt	43.55	3.24	64,417	209
V_2O_5 powder	39.34	3.29	121,580	400

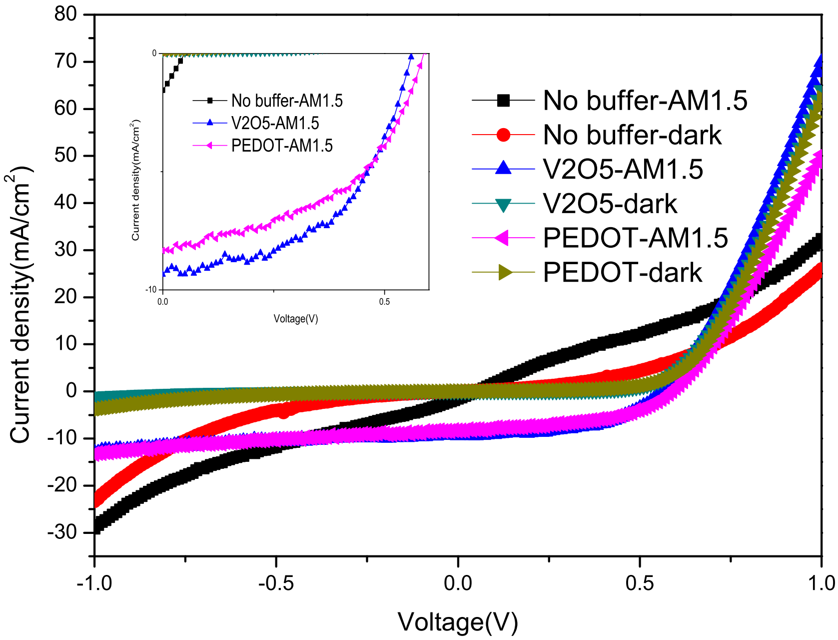

Fig. 5. Current density versus bias voltage curve of devices with and without V_2O_5 nanostructure, the inset is the enlarged part of the curve from 0 to 0.6 V.

short time constant of the nanobelt buffer layer mainly comes from the low charge transport resistance. Therefore, V_2O_5 nanobelt buffer layer can facilitate the charge transport between the two electrodes while reducing the recombination process to increase J_{sc}. The rougher surface of the V_2O_5 nanobelt film as shown in Fig. 1 could eventually increase charge passing area and thus could be another possible reason to boost J_{sc}.

The current density versus bias voltage characteristics of the photovoltaic devices without buffer layer, with 200 μg/mL V_2O_5 nanobelt and with PEDOT-PSS as buffer layer in dark and under irradiation of AM 1.5 100 mW cm^{-2} are compared in Fig. 5, showing that both buffered devices give significantly higher performance. The non-buffered devices illustrate a nearly symmetric *J–V* curve, indicating a large leakage current (~29 mA/cm^2 in dark and 23 mA/cm^2 under light). In the devices with V_2O_5 nanobelt as the buffer layer the leakage current are much lower (~1 mA/cm^2 in dark and 12 mA/cm^2 under light). Since the direction of the leakage current is reverse to that of the photocurrent, a lower leakage current leads to enhanced V_{oc} and *FF* and thus higher efficiency. The results in Fig. 5 clearly show that V_2O_5 nanobelt (200 μg/mL)-buffered solar cell improves *PCE* than that without such a buffer layer by 20 times and even has J_{sc} (9.35 mA/cm^2), *FF* (51.9%) and *PCE* (2.72%) higher than that (J_{sc}: 8.34 mA/cm^2, *FF*: 48.6% and *PCE*: 2.39%) of PEDOT-PSS-buffered polymer solar device fabricated with the same conditions in our lab. Very recently, Zilberberg et al.'s work demonstrates that a smooth V_2O_5 layer fabricated from a sol–gel process, which is relatively flat without nanowire or belt feature could also achieve similar performance to the PEDOT-PSS control device [24]. This may indicate that the sol–gel process could provide an approach to make a material with better charge transport or/and charge separation properties. We wonder whether a nanowire structure made from the sol–gel process could further improve the device performance. Experiments are planned and will be conducted in this lab. It is worthy of a note that the *PCE*s achieved in this work is lower than the common value of 3.0–5.0% very possibly due to that all the fabrications are carried out in air and it is in agreement with that reported by Wu et al. [33,34].

4. Conclusion

In conclusion, the nanostructure effect of V_2O_5 buffer layer on performance of polymer solar cells has been studied. V_2O_5 nanobelts are synthesized by a solution process and further used as the anode buffer layer. The V_2O_5 nanobelt-buffered device achieves *PCE* of 2.71%, which is much higher than that (1.08%) of V_2O_5 powder-buffered device. XRD results support that the V_2O_5 nanobelt buffer layer could promote the phase separation in the active layer for higher short circuit current. The impedance spectrum proves that V_2O_5 nanobelt buffer layer can significantly shorten the charge transport time in the active layer to reduce the charge recombination for higher J_{sc}. The V_2O_5 nanobelt-buffered solar cell also demonstrates higher *PCE* (2.71%) than that (2.39%) of PEDOT-PSS buffered device. We can argue that this work provides not only fundamental insights of the nanostructure effect on solar cell performance, but also a good substitute (V_2O_5 nanobelt) for PEDOT-PSS to improve the P3HT:PCBM solar cell performance.

Reference

[1] N.S. Sariciftci, D. Braun, C. Zhang, V.I. Srdanov, A.J. Heeger, G. Stucky, F. Wudl, Semiconducting polymer-buckminsterfullerene heterojunctions: diodes, photodiodes, and photovoltaic cells, Appl. Phys. Lett. 62 (1993) 585–587.

[2] G. Yu, J. Gao, J.C. Hummelen, F. Wudl, A.J. Heeger, Polymer photovoltaic cells: enhanced efficiencies via a network of internal donor-acceptor heterojunctions, Science 270 (1995) 1789–1791.

[3] M. Granstrom, K. Petritsch, A.C. Arias, A. Lux, M.R. Andersson, R.H. Friend, Laminated fabrication of polymeric photovoltaic diodes, Nature 395 (1998) 257–260.

[4] C. Gong, Q.L. Song, H.B. Yang, J. Li, C.M. Li, Polymer solar cell based on poly(2,6-bis(3-alkylthiophen-2-yl)dithieno-[3,2-b,2′,3′-d]thiophene), Sol. Energy Mater. Sol. Cells 93 (2009) 1928–1931.

[5] H. Yang, Q. Song, Z. Lu, C. Guo, C. Gong, W. Hu, C.M. Li, Electrochemically polymerized nanostructured poly(3,4-ethylenedioxythiophene)-poly(styrenesulfonate) buffer layer for a high performance polymer solar cell, Energy Environ. Sci. 3 (2010) 1580–1586.

[6] C. Gong, H.B. Yang, Q.L. Song, Z.S. Lu, C.M. Li, Solar cells made from polymers containing dithieno[3,2-b,2′,3′-d]pyrrole with different side chain lengths, Sol. Energy Mater. Sol. Cells 95 (2011) 969–973.

[7] S.M. Tuladhar, M. Sims, S.A. Choulis, C.B. Nielsen, W.N. George, J.H.G. Steinke, D.D.C. Bradley, J. Nelson, Influence of side chain symmetry on the performance of poly(2, 5-dialkoxy-p-phenylenevinylene): fullerene blend solar cells, Org. Electron. 10 (2009) 562–567.

[8] F. Nickel, A. Puetz, M. Reinhard, H. Do, C. Kayser, A. Colsmann, U. Lemmer, Cathodes comprising highly conductive poly(3, 4-ethylenedioxythiophene):poly(styrenesulfonate) for semi-transparent polymer solar cells, Org. Electron. 11 (2010) 535–538.

[9] W.L. Ma, C.Y. Yang, X. Gong, K. Lee, A.J. Heeger, Thermally stable, efficient polymer solar cells with nanoscale control of the interpenetrating network morphology, Adv. Funct. Mater. 15 (2005) 1617–1622.

[10] K. Kim, J. Liu, M.A.G. Namboothiry, D.L. Carroll, Roles of donor and acceptor nanodomains in 6% efficient thermally annealed polymer photovoltaics, Appl. Phys. Lett. 90 (2007).

[11] W.-J. Yoon, P.R. Berger, 4.8% efficient poly(3-hexylthiophene)-fullerene derivative (1:0.8) bulk heterojunction photovoltaic devices with plasma treated AgO_x/indium tin oxide anode modification, Appl. Phys. Lett. (9) (2008) 013306.

[12] H. Ma, H.-L. Yip, F. Huang, A.K.Y. Jen, Interface engineering for organic electronics, Adv. Funct. Mater. 20 (2010) 1371–1388.

[13] S. Bertho, W.D. Oosterbaan, V. Vrindts, J. D'Haen, T.J. Cleij, L. Lutsen, J. Manca, D. Vanderzande, Controlling the morphology of nanofiber-P3HT:PCBM blends for organic bulk heterojunction solar cells, Org. Electron. 10 (2009) 1248–1251.

[14] W.-S. Chung, H. Lee, W. Lee, M.J. Ko, N.-G. Park, B.-K. Ju, K. Kim, Solution processed polymer tandem cell utilizing organic layer coated nano-crystalline TiO_2 as interlayer, Org. Electron. 11 (2010) 521–528.

[15] A. Kumar, H.-H. Liao, Y. Yang, Hole mobility in optimized organic photovoltaic blend films obtained using extraction current transients, Org. Electron. 10 (2009) 1615–1620.

[16] S.-I. Na, S.-H. Oh, S.-S. Kim, D.-Y. Kim, Efficient organic solar cells with polyfluorene derivatives as a cathode interfacial layer, Org. Electron. 10 (2009) 496–500.

[17] S.C. Jain, T. Aernout, A.K. Kapoor, V. Kumar, W. Geens, J. Poortmans, R. Mertens, I–V characteristics of dark and illuminated PPV-PCBM blends solar cells, Synth. Met. 148 (2005) 245–250.

[18] K. Kawano, R. Pacios, D. Poplavskyy, J. Nelson, D.D.C. Bradley, J.R. Durrant, Degradation of organic solar cells due to air exposure, Sol. Energy Mater. Sol. Cells 90 (2006) 3520–3530.

[19] G. Li, C.W. Chu, V. Shrotriya, J. Huang, Y. Yang, Efficient inverted polymer solar cells, Appl. Phys. Lett. 88 (2006) 253503.

[20] C. Tao, S. Ruan, G. Xie, X. Kong, L. Shen, F. Meng, C. Liu, X. Zhang, W. Dong, W. Chen, Role of tungsten oxide in inverted polymer solar cells, Appl. Phys. Lett. 94 (2009) 043311.

[21] M.D. Irwin, D.B. Buchholz, A.W. Hains, R.P.H. Chang, T.J. Marks, p-Type semiconducting nickel oxide as an efficiency-enhancing anode interfacial layer in polymer bulk-heterojunction solar cells, Proc. Nat. Acad. Sci. 105 (2008) 2783–2787.

[22] V. Shrotriya, G. Li, Y. Yao, C.-W. Chu, Y. Yang, Transition metal oxides as the buffer layer for polymer photovoltaic cells, Appl. Phys. Lett. 88 (2006) 073508.

[23] J. Meyer, R. Khalandovsky, P. Görrn, A. Kahn, MoO_3 films spin-coated from a nanoparticle suspension for efficient hole-injection in organic electronics, Adv. Mater. 23 (2011) 70–73.

[24] K. Zilberberg, S. Trost, H. Schmidt, T. Riedl, Solution processed vanadium pentoxide as charge extraction layer for organic solar cells, Adv. Energy Mater. 1 (2011) 377–381.

[25] M. Kröger, Role of the deep-lying electronic states of MoO_3 in the enhancement of hole-injection in organic thin films, Appl. Phys. Lett. 95 (2009) 123301.

[26] M. Kröger, S. Hamwi, J. Meyer, T. Riedl, W. Kowalsky, A. Kahn, P-type doping of organic wide band gap materials by transition metal oxides: a case-study on Molybdenum trioxide, Org. Electron. 10 (2009) 932–938.

[27] J. Meyer, Electronic structure of Vanadium pentoxide: an efficient hole injector for organic electronic materials, J. Appl. Phys. 110 (2011) 033710.

[28] J.-S. Huang, C.-Y. Chou, M.-Y. Liu, K.-H. Tsai, W.-H. Lin, C.-F. Lin, Solution-processed vanadium oxide as an anode interlayer for inverted polymer solar cells hybridized with ZnO nanorods, Org. Electron. 10 (2009) 1060–1065.

[29] T. Zhai, H. Liu, H. Li, X. Fang, M. Liao, L. Li, H. Zhou, Y. Koide, Y. Bando, D. Golberg, Centimeter-long V_2O_5 nanowires: from synthesis to field-emission, electrochemical, electrical transport, and photoconductive properties, Adv. Mater. 22 (2010) 2547–2552.

[30] T. Erb, U. Zhokhavets, G. Gobsch, S. Raleva, B. Stühn, P. Schilinsky, C. Waldauf, C.J. Brabec, Correlation between structural and optical properties of composite polymer/fullerene films for organic solar cells, Adv. Funct. Mater. 15 (2005) 1193–1196.

[31] M. Campoy-Quiles, T. Ferenczi, T. Agostinelli, P.G. Etchegoin, Y. Kim, T.D. Anthopoulos, P.N. Stavrinou, D.D.C. Bradley, J. Nelson, Morphology evolution via self-organization and lateral and vertical diffusion in polymer:fullerene solar cell blends, Nat. Mater. 7 (2008) 158–164.

[32] P.A. Troshin, D.K. Susarova, Y.L. Moskvin, I.E. Kuznetsov, S.A. Ponomarenko, E.N. Myshkovskaya, K.A. Zakharcheva, A.A. Balakai, S.D. Babenko, V.F. Razumov, Impedance measurements as a simple tool to control the quality of conjugated polymers designed for photovoltaic applications, Adv. Funct. Mater. 20 (2010) 4351–4357.

[33] S. Wu, J. Li, Q. Tai, F. Yan, Investigation of high-performance air-processed poly(3-hexylthiophene)/methanofullerene bulk-heterojunction solar cells, J. Phys. Chem. C 114 (2010) 21873–21877.

[34] S.K. Hau, H.-L. Yip, N.S. Baek, J. Zou, K. O'Malley, A.K.Y. Jen, Air-stable inverted flexible polymer solar cells using zinc oxide nanoparticles as an electron selective layer, Appl. Phys. Lett. 92 (2008) 253301–253303.